Application of Thermoplastic Polyester Elastomer for Honeycomb Shock Absorbing Components

Takaya Kobayashi and Yasuko Mihara

Mechanical Design & Analysis Corporation

Katsuhisa Yamashita, Chisato Nonomura,
Katsuhiro Kodama, Yumiko Isogai, and Tomoko Kanaya

TOYOBO Co. Ltd.

Abstract: Thermoplastic polyester elastomer (TPEE) possesses the properties of both rubber and engineering plastic. The most important feature of this material lies in its ability to combine the superior repulsion elasticity and flexibility of rubber with the rigidity of engineering plastic. This enables it to exhibit durability against fatigue, even when exposed repeatedly to large deformation. The most remarkable feature of TPEE is such that it can realize material properties with very small strain rate dependency. The authors have had their ample experiences with applying TPEE to large damper members in the civil engineering structures, such as fenders surrounding the piers of bridges to absorb the impact energy caused by ship collisions and the aseismatic connectors built in bridge structures. This paper attempts to develop shock absorbing components of small sizes with light weight for automobile applications. Locating TPEE shock absorbers inside the crash box (members connecting the bumper system to the main body) may be thought as a typical application of the TPEE products. In order to achieve weight saving of the shock absorbing components, it is effective to utilize the buckling behaviors of thin walled structures. With regard to the buckling simulations of cylindrical shell structures, the authors have been working to develop analysis procedures for obtaining stable solutions utilizing the latest general-purpose finite element technology. This report shows that the experimental results could successfully be reproduced by applying the simulation technique to the honeycomb-shaped shock absorbing components. For realizing a desirable load-displacement relationship, this report also shows how to modify the shape of the components.

Keywords: Buckling, Crashworthiness, Honeycomb, Polymer.

1. Introduction

If a hollow member represented by a circular cylinder or square section tube is subjected to axial compressions, various types of buckling modes are observed. These buckling modes are classified into three types as follows:

- Generating slender column buckling
- Generating lobes (extensional and axisymmetric)
- Generating lobes (non-extensional and non-axisymmetric)

Buckling of slender columns is also called Euler's buckling. In this type of structures, when the maximum stress reaches the elastic limit, plastic hinges are formed to yield to the collapse of the column. The energy required for collapsing is relatively small compared to the energy needed to produce lobes or wrinkles. Since the shock absorbing components are required to be capable of absorbing most of the impact energy, it is necessary to prevent long slender members from buckling due to bending.

If the axial length of a hollow member is relatively short, lobes or wrinkles are induced on its wall surfaces due to buckling behavior. An initial lobe originates at the end of the member while the second, third, and successive lobes are formed with progressive folding sequentially. While these lobes are consecutively formed, the buckling load remains almost constant and the characteristics can be utilized for the shock absorbing components.

The occurrence of lobes is classified into two types: extensional deformation and non-extensional deformation as shown in Figure 1 [1]. Extensional deformation is accompanied with membrane strains. For example, in case of a circular cylinder, axisymmetric deformation modes appear carrying the circumferential membrane strains.

However, the generation of the membrane strains is associated with increase in the loads and, accordingly, the deformation mode is likely to shift to non-extensional deformation mode, which is associated with smaller loads (more stable on the energy aspect). In case of a circular cylinder, dimples or lobes occur circumferentially and the resultant deformation modes called diamond buckling appear.

extensional **non-extensional**

Figure 1. Buckling modes of hollow shells [1].

From the view point of impact energy absorption performance, the extensional deformation mode seems to be most advantageous since it sustains the highest buckling load among all possible buckling modes. However, it is so difficult to obtain such mode in a stable manner in practice, especially for thin walled members. In order to make extensional deformations to progress steadily, it is necessary for the hollow sections to have a relatively thick wall.

While buckling is in progress, buckling mode is likely to shift to non-extensional buckling. Furthermore, if the boundary conditions become worse, buckling mode may possibly shift towards the slender column buckling to yield to the collapse of the structure eventually. Accordingly, for establishing a practical design of the shock absorbing components, the design specification should be decided from the point of view not only on the magnitude of the absorption performance of the impact energy but also on the stabilization of the buckling modes.

The honeycomb-shaped shock absorbing components are expected to be light in weight and to perform high energy absorption. As these barrier components are composed of multiple cells, there is no possibility of inducing slender column buckling. Since each wall of the honeycomb components is shared by an adjoining cell, it is difficult for each cell to deform, thereby keeping its originally symmetrical section. Therefore, it is usual to develop lobes to make deformed cross-sections non-symmetrical.

Honeycomb products have a long history and for the buckling load under the progressive folding of lobes, an applicable formula, including the plastic region, has been given. However, under the recent demands for higher degree of performance, a more precise manner of controlling the characteristics of load-displacement is required by means of detailed adjustments of the specifications.

In particular, it is very important to make sure that the occurrence of desirable buckling mode is stable by giving some artificial initial imperfections. In this study, honeycomb-shaped shock absorbing components made of TPEE were examined through experiments and through the analysis of the findings of authors [2] in connection with the buckling simulations of cylindrical shells.

The analysis was conducted by applying the explicit dynamic analysis approach (Abaqus/Explicit, Version 6.11 [3]) and resultantly, a three-dimensional behavior of buckling modes was traced in good accuracy. These results were applied to the design of the shapes of the honeycomb shock absorbing components in order to improve the desired performance.

2. TPEE material properties

The molecular structure of TPEE is a block copolymer composed of crystalline rigid polyester (hard segment) and non-crystalline soft polyester or polyether (soft segment). The mechanical property of TPEE is different from each other depending on the composition ratio of the hard and soft segments and the molecular structure.

The TPEE used in this study has the trademark PELPRENE™ (TOYOBO Co., Ltd.), where Polybutylene Terephthalate (PBT) as a hard segment and Polytetramethylene ether glycol (PTMG) as a soft segment are employed. In accordance with the composition ratio of the hard and soft segments, four grades of TPEE are prepared with the respective names of P-70B, P-90B, P-150B and P-280B. The number assigned to each grade name corresponds to ISO hardness.

Dumbbell test specimen (Type 1A, ISO 37:2005), as shown in Figure 2, are cut out from an injection-molded flat plate. The most significant feature of TPEE, as applicable to the shock absorbing components, is its very small strain rate dependency. Even if TPEE is exposed to high speed impacts, it can demonstrate a stable bumper performance without inducing any large increase in the reaction force.

In this study, using an ordinary tensile test machine, elongation and load between the gauge lines were measured under the condition with the tensile rate of 5 mm/min - 50 mm/min. Further high rate tensile test is scheduled to be carried out in the next fiscal year. The nominal stress-nominal strain is shown in Figure 3. The test result for P-90B is shown as a typical case.

As seen obviously in the figure, the degree of strain rate dependency in the test result is so small. The material initially exhibited elastic behavior and was met by the yield stress at the magnitude of the strain with approximately 30%. Necking behavior did not occur up to the magnitude of the strain of 500% and the deformation in the gauge length was confirmed to be uniform.

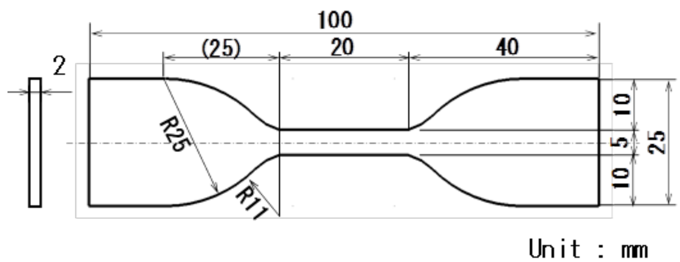

Figure 2. Tensile test specimen of TPEE (Type 1A, ISO 37:2005).

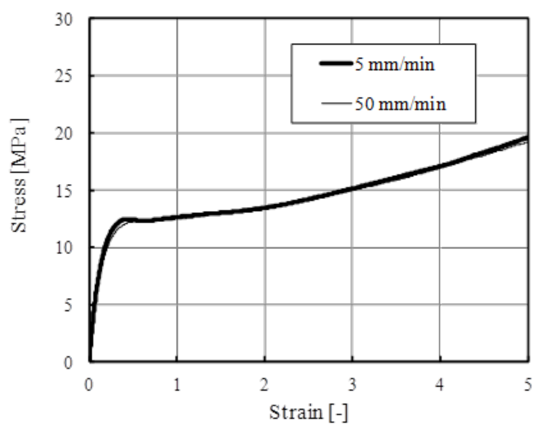

Figure 3. Nominal stress-nominal strain (TPEE, P-90B).

3. Findings from buckling of cylindrical shells

The elastic buckling of cylindrical shells under axial compression is regarded as a fundamental issue in the buckling of shell structures. The foundations of shell stability theory, it is generally agreed, were almost completely laid during the many studies of this subject [4]. The experimental achievements of Yamaki and his group (which are not limited to the case of axial compression) are covered in the literature [5]. Figure 4 and Figure 5 shows their typical results. All the cylinder models were constructed from Mylar (polyethylene terephthalate) film, and finished with the careful cleanup of geometric imperfections. Each model was fully fixed at both ends, and then compressed in the axial direction.

A typical deformation pattern of the test cylindrical shell is shown in Figure 4. This photograph illustrates the resultant deformation of the test cylinder compressed up to the axial shortening δ=0.606 mm. The cylindrical shell deformed in a sinusoidal form, of which the waves were observed to comprise axial half-waves of m=2 and circumferential full-waves of n=10. This non-axisymmetric buckling pattern, the so-called diamond buckling pattern, can be characterized by ridges in two inclined directions and furrows in circumferential directions. The combined length of all the furrows in each cross-section is nearly equivalent to the length of the original circle. Therefore, non-extensional deformation is achieved, and the cylindrical shell tends to exhibit the diamond buckling pattern.

The load-displacement curves in Figure 5 represent successive occurrences of buckling modes in which the first peak of 900N corresponds to the primary buckling. After the primary buckling, the deformed cylinder jumped to a stable bifurcation path with a non-axisymmetric shape, along with the dropping of the load. Subsequently, the cylindrical shell repeated consecutive snap-through buckling (secondary buckling) as the number of waves decreased one by one in the circumferential direction as the compression progressed.

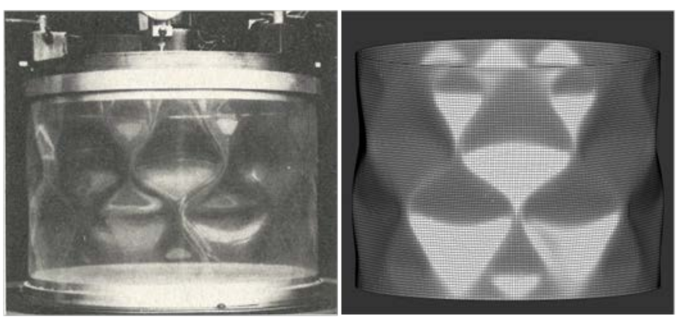

Experiment (Yamaki) **FEM (This study)**
r=100 mm, t=0.247 mm, L=113.9 mm, E=5560 MPa, ν=0.3

Figure 4. Deformation of Yamaki's test cylindrical shell under axial compression.

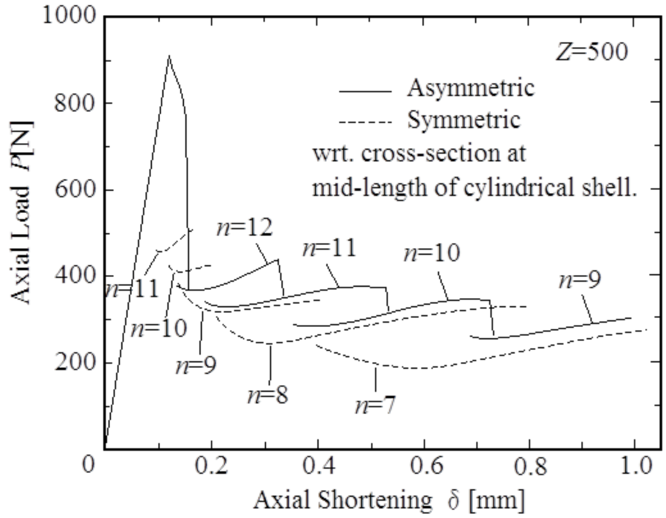

Figure 5. Load-shortening curves with mode-jumping in post-buckling region.

The number of circumferential waves was first found to be *n*=12, and was subsequently observed up to *n*=9, as shown in the figure. The primary purpose of the author's study [2] was to develop a seamless and numerically stable analysis procedure to simulate the whole buckling path of nearly perfect cylindrical shells, which exhibit buckling behavior that includes both imperfection-sensitive primary buckling and imperfection-insensitive secondary buckling accompanied with the mode jumping phenomenon.

Figure 6 shows the analysis results. The results most fully tracing to the experiments by Yamaki were obtained (Figure 5). Figure 6 also shows deformed shapes obtained from the analysis. The deformations are magnified in scale with the factors indicated in the figure. It is helpful to review the process of buckling by following the order of events.

At first, within the region “A” immediately before the occurrence of buckling, slightly out-of-plane deformation takes place. This shape is noted to be close to the axisymmetric buckling mode, with *m*=13， *n*=0 as indicated in the classical theory [6]. Near the primary buckling point “B”, some local buckles are initiated at the bottom portion of the cylinder, as is clearly indicated in the picture of the deformed shapes. The first single buckle generated becomes the starting point and, around it, buckles of similar shape are produced (Points C and D).

Next, the number of buckles sharply increases and, along with them, the load drops rapidly. At the same time, however, the number of waves rapidly decreases in both the circumferential and axial directions and then reaches Point E located on the stable path. The respective number of waves at this point is *m*=2 and *n*=12. The above-mentioned behavior, namely, rapid growth of the buckled deformation and the drop in the load within the interval from Point B to Point E happened in a very short time. This behavior was not captured in the experiments by Yamaki, while the same behavior was reported in the measurements by Esslinger [7] using high-speed photography.

When the deformation reaches the path with *n*=12 mode, the dropping of the load stops, and then the deformation progresses stably while the load slightly increases (Point E). However, as the compression advances, the cylinder again loses its stability and jumps to the path with *n*=11 (Point F), resulting in snap-through buckling (secondary buckling). This secondary buckling occurs one after another along with the progression of the deformation with *m*=2 remaining unchanged but with *n* decreasing one by one (Point E, F, G, and H). This type of mode jumping takes place toward a stable path on which the load is lowered and the slope is positive [8].

The above-mentioned report describes the result using static analysis (Abaqus/Standard). Figure 6 also shows the results from the explicit dynamic analysis (Abaqus/Explicit). Very little difference was found between them. From the viewpoint of the developments in the conventional research work, it is reasonable for us to consider that the essential nature of the post-buckling behavior can be regarded as a static problem, even though it may be possible to raise some side issues such as the occurrence of overshooting in deformation due to the inertia effect.

In this study, both the static analysis with the artificial damping and the explicit dynamic analysis were applied. However, the reason for the task was to confirm the above-mentioned understanding, not to conduct the simulation for the dynamic effect itself, i.e., the release of local strain energy due to the inertia effect.

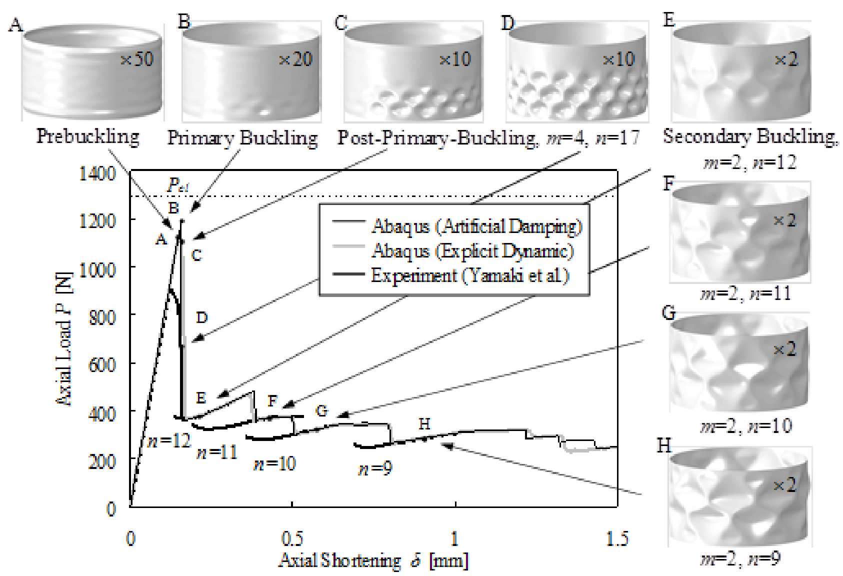

Figure 6. Results from artificial damping method and explicit dynamic analysis for Yamaki's experiment [2].

4. Study on three-cell honeycomb

With the purpose of examining the buckling features of the honeycomb components made of TPEE, experiments and analysis were performed for a simple structure assembled with three cells. Figure 7 shows the model shape. As shown in the figure, the tips of the model are chipped to provide partial cut-outs so that the resultant load-displacement performance can be improved. By designating the model without the cut-out as Case-1 and the other with the cut-out as Case-2, both of these cases were examined for comparison. The material used for these models was P-90B.

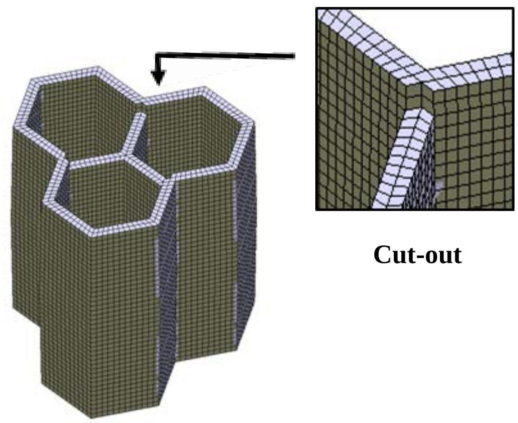

Figure 7. Three-cell honeycomb test model.

The honeycomb model was a product formed by injection molding that had a relatively thick wall. Accordingly, as seen in Figure 8, buckling was initiated, triggered by a local deformation at the tip of the model. Such initial local deformation, as apparently observed from the figure, is recognized to be of extensional deformation pattern with mostly symmetrical hexagonal cross-sections. However, this deformation is finally transitioned into asymmetrical deformation pattern. The load-displacement curves are shown in Figure 9 (Case-1 without cut-out) and Figure 10 (Case-2 with cut-out). Since buckling began with nearly extensional deformation, the load takes its peak value at the initial stage of deformation.

With regard to the elastic buckling of honeycomb components subjected to axial compressions, Ashby *et al.* [9] propose Equation (1) to obtain the elastic critical load. This formula can be regarded as an extended form of the classical formula for the elastic buckling of a flat panel constrained at its two edges parallel to load direction (*e.g.* Timoshenko [6]). P_{cr} denotes the elastic critical load per panel and, for the honeycomb model with three cells as shown in Figure 7, is assembled with totally 15 panels.

$$P_{cr} = \frac{KE}{(1-\nu^2)} \frac{t^3}{l} \tag{1}$$

Where

P_{cr}: Elastic critical load per panel,

E: Young's modulus (154 MPa),

ν: Poisson's ratio (0.4),

l: Panel width (Edge length of honeycomb segment, 25 mm),

b: Panel height (Honeycomb height, 100 mm),

t: Wall thickness (4.3 mm)

K: Constraint factor

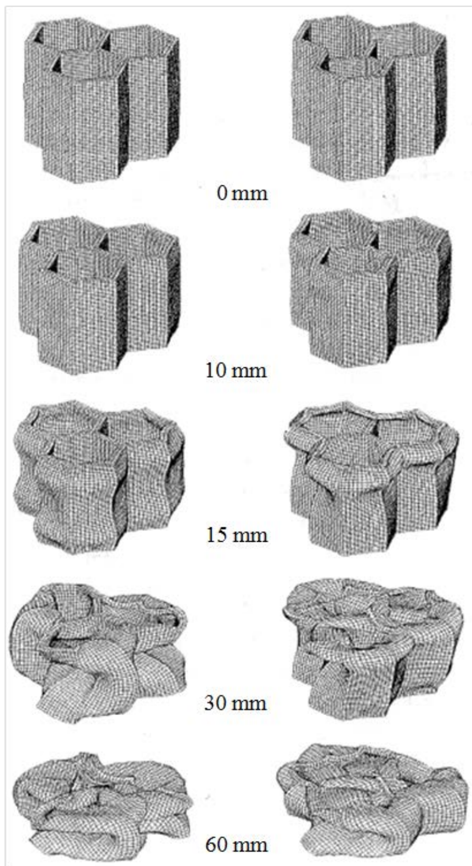

Case-1 without cut-out **Case-2 with cut-out**

Figure 8. Deformed shape under axial compression.

The constant K is a factor representing the constraint conditions at the top and bottom end of the honeycomb. If the edge can freely rotate without any constraints—for example, if a panel's height b is sufficiently tall compared to its width l (e.g., $b>3l$), then $K=2$. If all rotational degrees of freedom are fully constrained, then $K=6.2$. For honeycomb structures, Ashby *et al.* suggest to approximate this K as an intermediate value of $K=4$. In this study, we assumed that $K=3$ because the wall is relatively thick.

By calculating based on this approximation, the elastic critical load of the three-cell model is given as about 26 kN, which closely agrees with the peak value at the initial stage of approximately 25 kN as derived from the analysis of Case-1(shaped without any cut-out) as shown in Figure 9.

The existence of the initial peak load has the potential to cause excessive reaction forces at the moment of the crash impact. Therefore, an attempt was made to reduce the peak load on the model of Case-2 by giving cut-outs at the tips of the honeycomb assembly. As shown in Figure 10, the resultant peak load could be reduced to as far as 20kN.

The peak load by the elastic critical load corresponds to the primary buckling. For the buckling of cylindrical shells subjected to axial compressions, it is pointed out that the primary buckling load not only corresponds to the axisymmetric buckling modes but also represents the critical load of the non-axisymmetric buckling modes with sinusoidal waves in both the circumferential and the axial directions [2].

For the case of honeycomb components, because the load obtained by Equation (1) is a solution extended from the buckling formula for a flat plate panel, it may not be meaningful to argue whether or not the deformation modes actually generated are close to axisymmetric pattern. In fact, from a comparison between Case-1 and Case-2, the peak loads are noted to vary. It does not mean, however, that the existence of the peak itself vanishes. Giving cut-outs can be understood properly as such that it allows more free rotation at the ends, such that the constraint factor K can be reduced.

After passing the peak of the primary buckling mode, the honeycomb enters the post-buckling region and thereby the load sharply drops. This behavior is similar to the case of the cylindrical shells. In the case of the cylindrical shells, there are multiple stable paths that are accompanied by non-axisymmetric deformation modes on a load-displacement plane and their load level is remarkably lower than the critical load of the primary buckling mode. Then, the cylindrical shell is led to one of its stable paths along with losing loading. From a resultant displacement of 30mm in Figure 8, it is observed that the honeycomb is led to non-axisymmetric deformation pattern, which is different from the primary buckling mode.

However, since the honeycomb models in this study have relatively thicker wall, the yield of TPEE takes place in accordance with the progress of deformations. Therefore, the gradient of the load drop becomes moderate and any behavior with snap-through as exhibited in elastic shells is not seen. Ashby *et al.* [9] derived Equation (2) for the collapse load of the honeycomb components accompanied with yielding by approximating it with the plastic hinges of panels. The load given by this formula is 9.6 k N.

$$P_y = \frac{1}{2}\pi\sigma_y t^2 \tag{2}$$

Where

P_y: Yield load per panel,

σ_y: Yield stress (22 MPa)

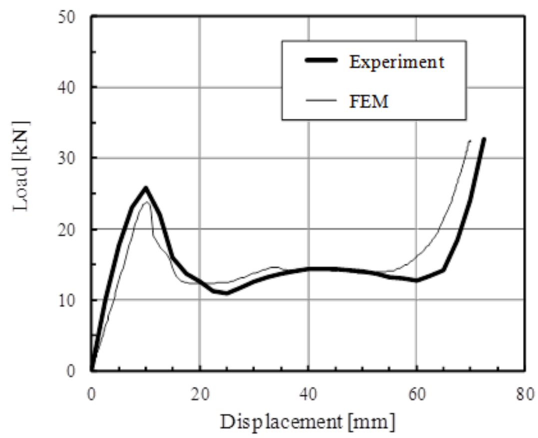

Figure 9. Load-displacement curves (Case-1 without cut-out, three-cell honeycomb).

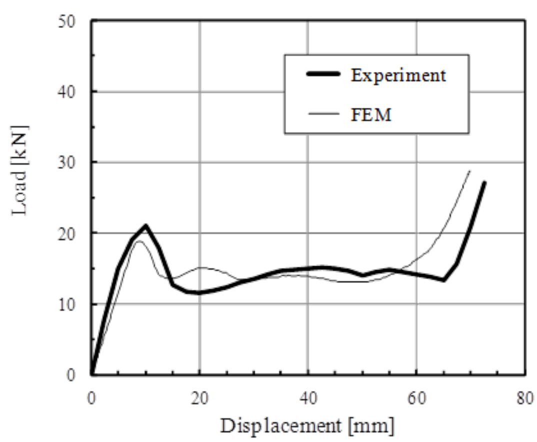

Figure 10. Load-displacement curves (Case-2 with cut-out, three-cell honeycomb).

Since the bending moment borne by plastic hinges is constant irrespective of bent angles, the load after the honeycomb walls are entirely yielded is expected to be kept constant. In Figure 9 and Figure 10, the magnitude of the load after the primary buckling indicates that it is mostly constant with a value of about 10 kN. As obviously noted from these figures, this plateau region corresponds to the constant load spans of over the range of 20 to 60mm of the displacements. This coincides with the result of the simplified formula assuming plastic hinges. When a structure is buckled accompanied with yielding, its load capacity is not only dependent on the paths determined from the elastic stability theory but also on the yield stress.

As the honeycomb components are produced through the injection molding process, the distribution of the initial draft exists over the wall surfaces of the honeycomb components. It means that the wall thickness in the mid-height of the honeycomb components is thicker than those at the ends of the components. It results to having the load over the plateau region not perfectly flat. Therefore, nominal drafts were given to the analysis models.

The height of the honeycomb used in this study is 100mm. After the load curve indicates a plateau and the compression ratio exceeds 60%, the walls of the honeycomb model begin to be folded progressively, resulting to self-contact and the load turns to increase. The honeycomb component can be effective as the shock absorber up to the plateau region.

As the real events of collision between automobiles are not limited to head-on collisions, further studies for the compression due to the offset crash are definitely needed. In particular, the initial peak load is considered to be largely affected by the direction of crashes. The peak loads must be dependent on the numbers and shapes of the honeycomb components. These studies are planned to be made with real-world design parameters.

Analysis was carried out using Abaqus/Explicit. For the buckling problems of thin-walled cylindrical shells, findings were taken using shell elements. However, for problems associated with relatively thick walls like the honeycomb components in this study, local deformations of the tips, as represented by the constraint factor K in Equation (1), provide great influences. It is also necessary for the wall surfaces to describe precisely their self-contact behaviors. Accordingly, applying solid elements is considered to be advantageous. In this study, element type C3D8R was used.

This element type is provided with formulation of the reduced integration scheme and, accordingly, its use is advantageous in terms of computational time. Since the occurrence of hourglass modes is appropriately suppressed, no difficulty was encountered. In order to describe plasticizing in the wall surfaces, meshing with four layers is given in the direction of the wall thickness.

5. Study on multi-cell honeycomb

A honeycomb model, with the number of cells increased to 18, was examined. Figure 11 shows its shape. Similar to the three-cell test model, the model without cut-outs is designated as Case-3 and the other with cut-outs is designated as Case-4. The experimental results of the load displacement are shown in Figure 12 and Figure 13.

Compared with the three-cell model, the peak load at the primary buckling is smaller than the value proportional to the numbers of cells (six times). In particular, for Case-4 with cut-outs, the peak value is not evidently identified. Some possibility is suggested as such that increasing the numbers of cells tends to reduce the constraint factor *K*, but further investigations are necessary to clarify this phenomenon. Currently, some simulations are being conducted. The loads in the plateau region resulted to values that are proportional to the number of cells, indicating that yielding in the wall is a stable phenomenon. The CPU time was around several hours on an average PC.

Figure 11. 18-cell honeycomb test model.

6. Conclusions

With the aim to develop new light-weight shock absorbing components, experimental and analytical investigations were carried out for the honeycomb components made of thermoplastic polyester elastomers (TPEE). Buckling behaviors of the honeycomb components were examined by evolving the findings of the cylindrical shells that were subjected to axial compressions.

The following is a summary of the consequent findings from this study and the future scopes for further studies:

- It is found from the TPEE tensile tests that any remarkable rate dependencies are not exhibited at least within the low testing rate range. Further verifications that carry out the higher rate tensile tests are planned to be continued.
- The low rate compression tests were carried out and those results were compared with the simulation results. The simulations that employed solid elements to include effects from the behaviors of the component tips are recognized to be practically meaningful.
- For the multi-cell honeycomb components, more detailed studies are needed. Additionally, we need to obtain new findings and knowledge in connection with the offset crashes and the high speed impacts.

- Further high speed material tests and compression tests for honeycomb structures are currently under planning. Their results and findings will be reported in the near future.

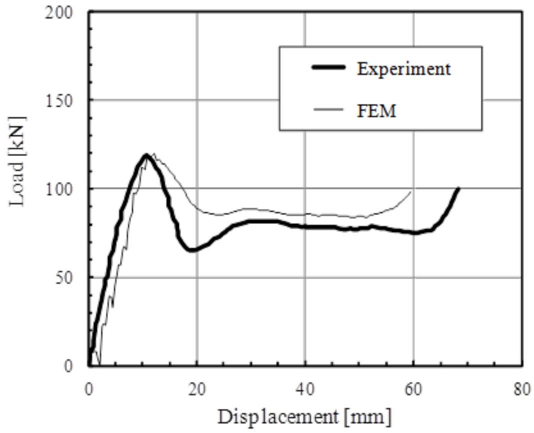

Figure 12. Load-displacement curves (Case-3 without cut-out, 18-cell honeycomb).

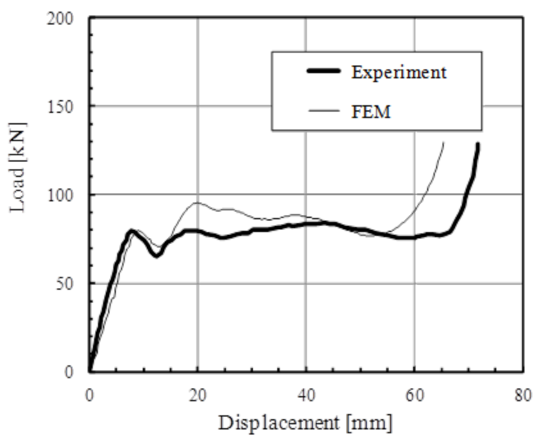

Figure 13. Load-displacement curves (Case-4 with cut-out, 18-cell honeycomb).

7. References

1. Jan Blachut, The University of Liverpool, http://shellbuckling.com/presentations/others/pages/page_135.html

2. Kobayashi, T., Mihara, Y., Fujii, F., "Path-tracing Analysis for Post-buckling Process of Elastic Cylindrical Shells under Axial Compression", Thin-Walled Structures, 61: 180-187,2012.
3. Abaqus Users Manual, Version 6.11, Dassault Systems Simulia Corp., USA, 2011.
4. Teng, J. G., Rotter, J. M., Buckling of Thin Metal Shells, Spon Press, UK, 2004.
5. Yamaki, N., Elastic Stability of Circular Cylindrical Shells, North-Holland, Netherlands, 1984.
6. Timoshenko, S.T., Gere, J. M., Theory of Elastic Stability, 2nd ed., McGraw-hill, New York, 1961.
7. Esslinger, M., "Hochgeschwindigkeitsaufnahmen von Beulvorgang dunnwandiger, axialbelasteter Zylinder", Der Stahlbau. 39 (3): 73-76, 1970.
8. Fujii, F., Noguchi, H., Ramm, E., "Static Path Jumping to Attain Postbuckling Equilibria of a Compressed Circular Cylinder", Computational Mechanics, 26 (3): 259-266, 2000.
9. Gibson, L. J., Ashby, M. F., Cellular Solids: Structure and Properties, 2nd ed., Cambridge University Press, UK, 1999.